(The final manuscript (Y/M09012))

Measurements of Critical Heat Flux and Liquid-Vapor Structure near the Heating Surface in Pool Boiling of 2-propanol/Water Mixtures

Hiroto Sakashita [a,*], Ayako Ono [a] and Yuta Nakabayashi [a]

[a] Division of Energy and Environmental Systems, Graduate School of Engineering, Hokkaido University, North 13 West 8, Kita-ku, Sapporo 060-8628, Japan

* Corresponding author. Tel.: +81 11 706 6664, Fax.: +81 11 706 6664

E-mail address: saka@eng.hokudai.ac.jp

Abstract

Saturated pool boiling of 2-propanol/water mixtures on a 12mm diameter horizontal disk under atmospheric pressure was investigated. The CHF of the mixtures increased up to 1.7times the CHF of water at 3.0 to 4.7 mol% concentrations of 2-propanol. To examine the mechanism of the CHF enhancement in the mixtures, liquid-vapor structures close to the heating surface were measured using a conductance probe. It was found that in the boiling of the mixtures, liquid-vapor structures show strong non-uniformity in the radial direction of the heating surface. The void fractions at 0.1mm to 1mm above the heating surface are small at the central region and large near the periphery of the heating surface. The liquid layer between the vapor mass and the heating surface is considerably thicker than that of water at the central region and becomes thinner near the periphery of the heating surface. This thicker liquid layer is likely to be the cause of the CHF enhancement in the 2-propanol/water mixtures.

Key Words: Critical heat flux, Binary mixtures, Pool boiling, Conductance probe, Macrolayer

1. Introduction

It has been known that the CHF in pool boiling of water is often enhanced when small amounts of alcohols or ketones are added to the water. Van Wijk et al. [1] carried out experiments of boiling on 0.2 mm horizontal wires with aqueous binary mixtures of various alcohols, acetone, and methyl-ethyl-ketone, and reported that the CHF was enhanced 1.7 to 3.4 times compared to the CHF of water. Kutateladze et al. [2] measured the CHF of ethanol/water mixtures on a 0.5 mm horizontal wire and obtained a 1.7 times increase in the CHF relative to the water at a 9 mol% ethanol addition. Reddy and Lienhard [3] measured the CHF of ethanol/water mixtures for horizontal wires with wire diameters from 0.51 to 2.18mm and obtained CHF enhancements up to 1.2 to 1.3 times the CHF of water with wires thinner than 1.02mm in diameter. Fujita and Bai [4] carried out experiments with methanol/water and ethanol/water mixtures on 0.5 mm horizontal wires and observed a 1.9 times enhancement of the CHF. Inoue et al. [5] also carried out an experiment with ethanol/water mixtures on 0.3mm horizontal wires to obtain a 1.8 times enhancement of the CHF.

As for the CHF of flat surfaces, Bonilla and Perry [6] used 67mm and 90mm diameter horizontal disks and reported 1.1 times enhancement for ethanol/water mixtures and 1.2 times for 1-buthanol/water mixtures, compared to the CHF of water. Kutateladze et al. [2] obtained a 1.2 times increase in the CHF in the boiling of ethanol/water mixtures on a 6mm wide upward facing rectangular surface. McGillis and Carey [7] carried out experiments with a 12.7mm×12.7mm upward facing square surface at pressures lower than 10kPa. They obtained a 1.7 times enhancement in CHF for methanol/water mixtures and 2.1 times for 2-propanol/water mixtures.

In theoretical studies, Reddy and Lienhard [3] examined the cause of CHF enhancement based on increases in effective subcooling. In the boiling of mixtures, concentration of more volatile component around the vapor bubbles becomes lower than that of the bulk liquid. As a result, the temperature at the liquid-vapor

interface becomes higher than the saturation temperature (bubble point temperature) of the bulk liquid. This situation is similar to subcooled boiling with a single component fluid, and this is the cause of the CHF increases. Based on this idea, Reddy and Lienhard [3] proposed the following empirical correlation based on their own data from horizontal wires [3].

$$\frac{q_{CHF}(1+0.1x)}{q_{CHF,SL}} = (1-0.170Ja_e^{0.308})^{-1} \quad (1)$$

$q_{CHF,SL}$ is the critical heat flux for saturated boiling on horizontal wires proposed by Sun and Lienhard [8], Ja_e is the Jakob number defined by Reddy and Lienhard [3] to express the effect of subcooling:

$$Ja_e = \frac{\rho_f C_{pf}(T_g(x)-T_b(x))}{\rho_g h_{fg}} \quad (2)$$

(Definitions of $T_g(x)$ and $T_b(x)$ are shown in Fig.3). The predicted values of equation (1) agree with the CHF data of ethanol/water mixtures by Reddy and Lienhard [3] over a wide range of ethanol concentrations.

Another explanation of CHF enhancement is based on the Marangoni effect occurring at the liquid-vapor interface. In the boiling of binary mixtures, evaporation of the more volatile component from the liquid-vapor interface is more intensive near the heating surface, and hence, concentration of the more volatile component in the liquid phase adjacent to the interface decreases toward the heating surface. This yields a surface tension gradient according to the concentration distribution along the liquid-vapor interface. For the positive mixtures in which more volatile component has lower surface tension, therefore, Marangoni convection is induced toward the heating surface, and this may cause the CHF enhancement. Hovestreudt [9] adopted a bubble merger model as the CHF model, and assumed that Marangoni convection around a bubble inhibits the coalescence of bubbles and therefore enhances the CHF. Based on this idea, Hovestreudt [9] proposed the following parameter relating to the CHF of binary mixtures as

$$M = (x-y)\cdot d\sigma/dx \quad (3)$$

Fujita and Bai [4] considered that the flow induced by the Marangoni effect along the surface of growing bubbles or thin liquid film beneath bubbles retards coalescence of bubbles or dryout of the heating surface, resulting in CHF enhancement. Based on this assumption, Fujita and Bai [4] proposed a following empirical correlation using their own data of the CHF measured with a 0.5mm diameter horizontal wire.

$$q_{CHF} = q_{CHF,Z}\left(1-1.83\times10^{-3}\frac{|Ma|^{1.43}}{Ma}\right)^{-1} \tag{4}$$

In equation (4), Ma is the Marangoni number defined by Fujita and Bai [4] as

$$Ma = \frac{\Delta\sigma}{\rho_f \nu_f{}^2}\left\{\frac{\sigma}{g(\rho_f-\rho_g)}\right\}^{1/2} Pr_f \tag{5}$$

In equation (5), $\Delta\sigma$ is the difference in the surface tension at the boiling point and the dew point (The two points are shown as A and B in Fig.3). McGillis and Carey [7] also considered the Marangoni effect as the cause of the CHF enhancement. They used the CHF model by Zuber and assumed that liquid supply toward the heating surface due to Maraogoni convection at the interface of the vapor columns enhances the CHF. Based on these assumptions, they proposed the following correlation.

$$q_{CHF} = q_{CHF,sf}\left[1+c_m\left|\frac{1}{\sigma}\cdot\frac{\partial\sigma}{\partial x}(y-x)\right|\right]^{1/4} \tag{6}$$

where c_m is an empirical constant and decided on a value of 1.4 to fit the data. Predicted values of equation (6) agree fairly well with the CHF data of methanol/water and 2-propnaol/water mixtures by McGillis and Carey [7] and the data of ethanol/water mixtures by Reddy and Lienhard [3] in a wide range of concentrations. Yagov [10] proposed a CHF model for a single component fluid, where the CHF is triggered by irreversible enlargement of the dry area on a heating surface. For binary mixtures, he assumed that the liquid supply from the surrounding liquid film (Yagov termed it 'a macrofilm') to a dry area due to

Marangni effects retards the irreversible enlargement of the dry area, and hence enhances the CHF. Based on this assumption, Yagov [10] proposed the following correlation.

$$q_{CHF} = q_{CHF,sf}\left(1 + k_m \frac{\Delta\sigma}{\sigma}\right) \tag{7}$$

$\Delta\sigma$ is the difference in the surface tension at the dew point and the bubble point (points A and B in Fig.3); and k_m is a constant that Yagov gives the value of unity. Equation (7) agrees fairly well with the available CHF data for ethanol/water and methanol/water mixtures over a wide range of concentrations.

As above, there are a number of studies on the CHF of binary mixtures, but the mechanism of the CHF enhancement has not been established. One main reason is that there is no information of liquid-vapor structures in the vicinity of heating surfaces at high heat fluxes during boiling of mixtures. Considering that the trigger for the CHF is closely related to the phenomena occurring close to the heating surface, such information is vital to establish the CHF mechanism of the mixtures. This study focuses on the CHF of 2-propanol/water mixtures in pool boiling on an upward-facing heating surface under atmospheric pressure. The CHF was measured and the liquid-vapor structures in the vicinity of the heating surface were closely examined based on measurements with a conductance probe in the range of 2-propanol concentrations of 0 to 7 mol% (mass fraction of 0 to 20%). For comparison, an experiment with an aqueous surfactant (SDS) solution was carried out to examine differences in the liquid-vapor behaviors. Through these measurements, reasons why the CHF of water is enhanced by adding 2-propanol are discussed.

Nomenclature

C_p Specific heat

g gravitational acceleration

H_{fg} latent heat of evaporation

h height from heating surface

Ja_e modified Jakob number , defined in Eq.(2)

M parameter defined in Eq.(3)

Ma Marangoni number defined in Eq.(5)

Pr Prandtl number

q heat flux

q_{CHF} critical heat flux

$q_{CHF,sf}$ critical heat flux of single fluid

$q_{CHF,SL}$ critical heat flux on wired by Sun and Lienhard

R radial position measured from the center of heating surface

T temperature

T_b saturation temperature (bubble point temperature)

x concentration of more volatile component in liquid phase

y concentration of more volatile component in vapor phase

Greek symbols

ΔT_{sat} surface superheat

$\Delta\sigma$ surface tension difference

δ_l macrolayer thickness

ν kinematic viscosity

σ surface tension

ρ density

Subscripts

f liquid

g vapor

2. Experimental

2.1 Experimental apparatus

The experiments were carried out in saturated pool boiling under atmospheric pressure. Fig.1 shows the experimental apparatus. The heating surface is the upper end of a cylindrical copper block and the diameter is 12mm. A 0.5mm thick stainless steel flange was silver soldered around the copper heating surface. The surfaces of the copper and the surrounding flange were machined to be flush, and then Ni was plated over the two surfaces to avoid nucleation of bubbles at the interface between the copper surface and the flange. The surface heat flux and the surface superheat were determined with two 0.5mm diameter thermocouples, which were embedded in the copper block 4 and 12mm below the surface. The boiling vessel is made of Pyrex glass with an inner diameter of 150 mm, and is surrounded by a water jacket to reduce distortions of video images when observing the boiling behaviors with high speed video (this water jacket is not depicted in Fig.1).

Liquid-vapor behaviors close to the heating surface were measured with a conductance probe. The measurement system with the conductance probe is described in detail in [11]. The tip of the conductance probe was thinned to less than 5μm by electro-polishing. An AC voltage of 24kHz, the resonance frequency of the measurement circuit, was applied between the conductance probe and the heating surface. The conductance probe was connected to a three-dimensional moving stage with an accuracy of 0.5μm in the vertical direction and 10μm in the horizontal direction. During the measurements with 2-propanol/water mixtures, KCl (potassium chloride) was added to increase the electro conductivity of the mixtures. The concentration of KCl was less than 100ppm and changes in the surface tension as well as other thermo-physical properties of the mixtures by adding the KCl were negligibly small.

Examples of raw signals from the probe and the converted digitized signals are shown in Fig.2, where a high voltage of the raw signal shows that the tip of the probe is in contact with vapor and a low voltage that it is in contact with liquid. In this paper, a digitized binary signal with high-level is termed a pulse and its

width as the pulse width.

2.2 Phase equilibrium and surface tension of 2-propanol/water mixtures

Fig.3 shows the phase equilibrium of 2-propanol/water mixtures and the surface tension of mixtures at the saturation temperature (bubble point temperature). The surface tension was estimated from an empirical correlation by Hoke and Chen [12], they measured the surface tension of the 2-propanol/water mixtures in a wide range of concentrations and temperatures. The surface tension drastically decreases with increasing concentration in the low concentration region. It is, therefore, expected that a strong Marangoni effect may be induced when a concentration gradient is formed along the liquid-vapor interface in a bulk liquid with low concentrations of 2-propanol.

3. Results and Discussion

3.1 Boiling curves and critical heat fluxes

Fig.4 shows the boiling curves for water and 2-propanol/water mixtures. The boiling curve of water lies close to the results predicted with the correlation for water by Stephan and Abdelsalam [13]. The boiling curves of 2-propanol/water mixtures shift toward higher superheat with increasing concentrations of 2-propanol, showing a deterioration of the boiling heat transfer by adding the alcohol, similarly to results of previous studies.

Fig.5 shows the CHF measured when varying the concentration of 2-propanol. The data scatter somewhat, but the CHF is most enhanced at around 3.0 to 4.7 mol% of 2-propanol concentration; the enhanced ratios of CHF vs. water are 1.61-1.69 at 3.0 mol% and 1.54-1.72 at 3.9-4.7 mol%. Fig.5 also shows the results predicted with equation (1) by Reddy and Lienhard, equation (6) by McGillis and Carey, and equation (7) by Yagov. Here, the $q_{CHF,SL}$ in equation (1) and $q_{CHF,sf}$ in equations (6) and (7) were calculated with the following Kutateladze-Zuber type correlation by using the properties of the mixtures.

$$q_{CHF} = C \cdot \rho_g^{1/2} H_{fg} \left[g\sigma\left(\rho_f - \rho_g\right)\right]^{1/4} \quad (8)$$

The constant C is determined as 0.177, as the predicted CHF of water with equation (8) agrees with the averaged value of CHF for water measured here, 1.5MW/m^2. Comparison with equation (4) by Fujita and Bai [4] was not made because the thermal conductivity of the 2-propanol/water mixtures included in Pr_f in equation (5) was not estimated. The magnitudes of the peak CHF are close to each other, but the tendencies of the changes in CHF with the concentration are different for the present data and the predictions.

3.2 Observation of the boiling behaviors

Fig.6 shows the appearance of the boiling for water and 3.0 mol% of 2-propanol/water mixture. At low heat fluxes (the isolated bubble region) in Fig.6-(a) and (b), it is observed that the departure diameter of the bubbles becomes smaller and the number of nucleation sites increases by addition of 2-propanol. At high heat fluxes in Fig.6-(c) and (d), large vapor masses covering the heating surface completely are formed with both water and the 2-propanol/water mixture. For the 3.0 mol% of 2-propanol/water mixture, the large vapor masses begin to form at a heat flux around 1MW/m^2. Above this heat flux, the high-speed video records with 2000fps show that many finer bubbles are generated on the heating surface just after the detachment of the preceding vapor mass, then immediately coalesce to form a large vapor mass. Once the large vapor mass is formed on the heating surface, there are few distinct differences in the boiling appearance of water and 2-propanol/water mixtures in the range of concentrations up to 7.0 mol%.

3.3 Void fraction distributions in vertical and radial directions

Figs.7 and 8 show the vertical distributions of time averaged void fractions for water and a 2-propanol/water mixture (3.0 mol%) measured at the center of the heating surface. For both water and mixture, the void fraction decreases

closer to the heating surface where it reaches zero, suggesting the existence of a liquid layer on the heating surface. However, there are considerable differences in the void fraction profiles of water and the 2-propanol/water mixture. Comparing at similar heat fluxes (1.25MW/m^2 for water and 1.23MW/m^2 for the mixture), the void fraction for the 2-propanol/water mixture begins to decrease further from the heating surface (h is about 2.5 to 3mm) and has considerably lower values than water in the h<1mm region. With increasing heat flux, the void fraction profiles of the 2-propanol/water mixture tend to approach those of water.

Figs.9 and 10 show the radial distributions of the void fractions, which were measured by traversing the probe horizontally along the centerline of the heating surface. The heat fluxes are 1.3MW/m^2 for water and 1.5MW/m^2 for the 2-propanol/water mixture (3.0mol%). There are noteworthy differences in the radial distributions. In Fig.9, for water, the void fraction distributions at h≥0.2mm are almost flat although the void fractions are a little higher near the periphery of the heating surface, showing that the heating surface is uniformly covered with vapor masses in the region of h≥0.2mm. In Fig.10, for the 2-propanol/water mixture, the void fractions at h=1mm or nearer fall in the central region of the surface and reach about 10% at h=0.5mm and 20% at h=1mm. At 2mm, the void fractions in the central region rise to almost the same value as those of water.

The axial distributions of the void fractions in Fig.8 measured at the center of the heating surface for the 2-propanol/water mixture are results reflecting these trends of the radial void fractions shown in Fig.10.

3.4 Liquid layer thickness formed beneath vapor masses

Ono and Sakashita [11] measured liquid-vapor behaviors near the horizontal heating surface using conductance probes in saturated and subcooled pool boiling of water under atmospheric pressure. They assumed that the region from the heating surface to the height below which the oscillation of the interface at the bottom of the vapor mass does not reach corresponds to the liquid layer (macrolayer), then it was possible to specify the thickness of the liquid layer from

the location where the vapor mass signals disappear. Here, the authors determine the liquid layer thickness based on the same assumptions.

First, an explanation of the term 'liquid layer'. A liquid-rich zone between vapor masses and a heating surface is usually termed a 'macrolayer', and the authors here also used the term 'macrolayer' in previous papers [11, 14]. As shown below, however, the liquid-rich zone is able to reach 1mm in thickness for 2-propanol/water mixtures, and it may be inappropriate to call this a macrolayer, which could be associated with a thin liquid-layer of tens to a few hundreds micrometers. This paper will, therefore, term the liquid-rich zone between vapor masses and heating surface a 'liquid layer', rather than a 'macrolayer'.

Details of the method to determine the liquid layer are represented in [11], and an outline of the method is shown next. The time-series data of the pulse signals were measured at various heights over the heating surface by moving the probe in the vertical direction (total number of pulses 4096 or 8192). Then, the pulses obtained at each height were classified into groups for every 2ms of pulse width, and the frequency of the appearance of pulses belonging to each pulse group was plotted. An example is shown in Fig.11 with the frequencies of appearance for the 4-6ms, 18-20ms, and 36-38ms pulse groups plotted against the distance from the heating surface. In Fig.11, the 18-20ms pulse group disappears at a height of about 0.2mm and the 36-38ms group at about 0.5mm. In such a manner, the height at which the frequency of appearance reaches zero was determined for each pulse group and is plotted in the top graph of Fig.12. Here, the height of disappearance of the pulse groups with very wide pulse widths is not included because the number of pulses for these groups are too few to show a smooth distribution of the frequency of appearance. The bottom graph of Fig.12 is the spectrum of pulse widths obtained 5.6mm over the heating surface. The vertical axis of the bottom graph of Fig.12 expresses the number of pulses counted within the measurement time. From the spectrum of the pulse widths, the pulses corresponding to the vapor masses were specified (in the bottom graph in Fig.12,

pulses from 19ms to 52ms were specified to correspond to the vapor masses). Finally, by comparing the two graphs, the location where the vapor mass signals disappear was determined. As shown in the top graph, the locations of the disappearance distribute over a wide range, and vapor masses with narrower pulse widths (with shorter hovering periods) are nearer to the heating surface. However, as the position of disappearance corresponding to the peak of the spectrum indicates the thickness of the liquid layer with the highest formation frequency, the average of several data points around the peak was considered to indicate the liquid layer thickness, and the nearest and the furthest locations of disappearance of the vapor masses (relative to the heating surface) were assumed to be the minimum and maximum thicknesses of the liquid layers.

The liquid layer thicknesses determined according to the above procedures are shown in Figs.13 to 15. In each figure, the symbols are the central peak values and the ends of vertical bars at each symbol indicate the minimum and maximum values. The macrolayer thicknesses with the empirical correlations proposed by Iida and Kobayasi [15] and Bhat et al. [16] for water at atmospheric pressure, and with the Haramura and Katto correlation [17] modified by Rajvanshi et al. [18] are also shown in Figs.13 to 15. Rajvanshi et al. [18] measured the macrolayer thickness for various liquids at atmospheric pressure using a conductance probe, and found that the data agree with twice the magnitude of the Haramura and Katto correlation [17] as

$$\delta_l = 0.0107 \frac{\sigma}{\rho_g} \left(\frac{\rho_g}{\rho_f} \right)^{0.4} \left(1 + \frac{\rho_g}{\rho_f} \right) \left(\frac{q}{\rho_g H_{fg}} \right)^{-2} \tag{9}$$

Fig.13 shows the variations of the liquid layer thickness obtained at the center of the heating surface with heat flux; the concentration of 2-propanol is 3.0 mol%. The data for water lie close to the predicted results with the previous correlations, however, the data for the 2-propanol/water mixture show a considerably thicker layer than the data for water, as could be expected from the vertical profiles of the void fractions (Fig.8). As the heat flux increases to approach

the CHF of the mixture, the liquid layer rapidly thins and approaches the extrapolated value of the water data. Fig.13 does not show the results of equation (6) by Rajvanshi et al. calculated with the physical properties of the 3.0 mol% of 2-propanol/water mixture, but equation (9) predicts the liquid layer of the mixture as 66% thinner than those for water, which is mainly due to reduction in the surface tension of the mixture as shown in Fig.3.

Fig.14 is the radial distributions of the liquid layer thicknesses for water and the 3.0 mol% of 2-propanol/water mixture. The heat fluxes are 1.25MW/m^2 for water and 1.5MW/m^2 for the mixture. The water data show flat distributions, and liquid layers with very similar thicknesses are formed at any radial location on the heating surface. On the other hand, the liquid layer thicknesses for the 2-propanol/water mixture show a strong non-uniformity: the liquid layer is very thick at the central region and becomes thin, reaching almost the values of water near the periphery of the heating surface. This non-uniformity of the liquid layer thickness results in the concave-shaped radial distributions of the void fractions at the heights of 0.2, 0.5, 1mm for the 2-propanol/water mixture shown in Fig.10. When the probe is located near the periphery of the surface with thin liquid layers, the probe tip rarely contacts with the liquid layer during the vapor mass hovering period. When the probe is located at the central region with thick liquid layers, the probe tip is in the liquid layer even when the vapor mass is hovering over the surface. This yields void fractions at h=0.2, 0.5, and 1mm that are large near the periphery and small near the central region of the heating surface.

Fig.15 is the liquid layer thickness measured at the center of the heating surface by varying the concentration of 2-propanol under similar heat flux (1.58 to 1.64MW/m^2) conditions. (The Rajvanshi correlation (9) predicts that the liquid layer thickness of the mixture decreases monotonously with increasing concentration of 2-propanol, a result not shown in Fig.15.) The liquid layer thickness increases with increasing concentration of 2-propanol, reaches a maximum at around 3.0 to 4.3 mol%, then tends to decrease with further

increases in the concentration. Interestingly, this tendency is similar to the dependence of the CHF on the concentration of 2-propnaol shown in Fig.5. The result in Fig.15 may suggest that the thicker liquid layer at central area of the heating surface causes the enhancement of the water CHF with added 2-propanol.

3.5 Measurements with aqueous solution of surfactant

As shown in Fig.6, the apparent difference of the boiling behavior between water and the 2-propanol/water mixtures is that the generated bubbles become smaller in the low heat flux region. Further, among the thermo-physical properties relevant to CHF, only the surface tension changes drastically by the addition of 2-propanol in the 0 to 7.0 mol% range of concentrations. We, therefore, examined whether the smaller bubbles and the reduction of the surface tension are causes of the differences in liquid-vapor structures between water and 2-propanol/water mixtures as shown in the preceding sections. To elucidate this, measurements with a surfactant aqueous solution were carried out, and sodium dodecylsulphate (SDS) was used as the surfactant. The concentration of SDS was selected as 600ppm as the surface tension of this SDS aqueous solution becomes almost the same as that of 3.0 mol% of 2-propanol/water mixture, at room temperature (about 40mN/m).

Fig.16 shows the boiling appearance for the SDS aqueous solution at low heat flux (0.19MW/m^2) and at high heat flux (1.42MW/m^2) close to the CHF. The appearances of the boiling with the SDS aqueous solution are similar to the boiling of 2-propanol/water mixture as shown in Fig.6-(b) and (d). At the low heat flux, bubbles detaching from the heating surface become fine and the number of nucleation sites increase compared with the water boiling shown in Fig.6-(a). On the other hand, at the high heat flux, there is formation of large vapor masses covering the heating surface.

Fig.17 shows the boiling curves for the SDS aqueous solution, water, and the 3.0 mol% of 2-propanol/water mixture. The boiling curve of the SDS solution is

at relatively low superheats, showing an enhancement of heat transfer. However, the CHF is little changed by adding SDS compared with water. Previous research reports that the addition of the surfactants enhances nucleate boiling heat transfer, and has little effect on the CHF [5, 19]. Fig.17 supports these findings.

Fig. 18 shows the vertical distribution of time averaged void fractions measured at the center of the heating surface. Here, the void fraction distribution for the SDS aqueous solution is entirely different from those of water and the 2-propanol/water mixture. The void fractions adjacent to the heating surface take extremely high values 90% or above, indicating that the heating surface always dries out and that there is no liquid layer under the vapor masses at the center of the heating surface. Fig.19 shows the radial distributions of the void fractions measured at 0.1mm and 0.5mm above the heating surface. In contrast to the profile of the 2-propanol/water mixture shown in Fig.10, the void fraction reaches nearly 100% at the central region and decreases sharply towards the edge of the heating surface.

These results may support the assumption mentioned at the end of the previous section that the thicker liquid layer at the central area of the heating surface causes the enhancement of the CHF of water. At the same time, it is also confirmed that the smaller bubbles and decrease in surface tension probably do not cause the thicker liquid layer and the differences in liquid-vapor structures of water and 2-propanol/water mixtures. There is still the possibility that the concentration of 2-propanol close to the heating surface differ greatly in the radial direction of the heating surface, which may lead to differences in boiling behaviors relevant to the liquid layer formation, such as nucleation site density, growth rate and detached frequency of primary bubbles, and coalescence process of bubbles.

4. Conclusions

The CHF and liquid-vapor behaviors near the heating surface were measured in pool boiling on an upward-facing heating surface for water,

2-propanol/water mixtures, and the surfactant (SDS) aqueous solution. The conclusions obtained by the present study may be summarized as follows:

(1) The CHF of 2-propanol/water mixtures are enhanced 1.7 times compared with the CHF of water at a 2-propanol concentration of around 3.0 to 4.7mol%.

(2) The liquid layer thicknesses of the 3.0mol% of 2-propanol/water mixture measured at the center of the heating surface are considerably thicker than those of water at heat fluxes close to the CHF of water.

(3) Liquid layer thicknesses of the 3.0mol% of 2-propanol/water mixture measured at 1.5MW/m^2 show a non-uniform distribution in the radial direction. Thicker at the central area and thinner near the periphery of the heating surface.

(4) The liquid layer thickness of 2-propanol/water mixtures measured at the center of the heating surface varies with the concentration of 2-propanol. With increasing concentration, the liquid layer thickness increases, reaches maximum at around 3.0 to 4.3mol%, then decreases. This tendency is similar to the dependence of the CHF on the concentrations of 2-propanol.

(5) Adding the surfactant (SDS) to water, the appearance of boiling becomes similar to that of the 2-propanol/water mixtures, but the CHF is not enhanced. The liquid-vapor structures of the SDS aqueous solution and the 2-propanol water mixtures are quite different.

(6) The formation of a thicker liquid layer at the central area of the heating surface may cause the CHF enhancement in 2-propanol/water mixtures.

(7) The reasons why the liquid-vapor structures are quite different among water, 2-propanol/water mixtures, and SDS aqueous solution remain unclear. Further study will be necessary to elucidate this.

References

[1] Van Wijk,W.R., Vos, A.S. and Van Stralen, S.J.D., Heat Transfer to Boiling binary liquid mixture, *Chem. Eng. Sci.* 5 (1956) 68-80.

[2] Kutateladze, S.S., Bobrovich,G.I., Goronin, I.I., Mamontova, N.N. and Moskvicheva, V.N., The Critical Heat Flux at the pool boiling of some binary liquid mixtures, *Proc. 3rd Int. Heat Transfer Conf.*, Chicago, 3(1966) 149-159.

[3] Reddy, R.P. and Liehnhard, J.H., The peak boiling heat flux in saturated ethanol-water mixtures, *Journal of Heat Transfer* 111(1989) 480-486.

[4] Fujita, Y. and Bai, Q., Critical heat flux of binary mixtures in pool boiling and its correlation in terms of Marangoni number, *Int. J. Refrig.*, 20-8(1997) 616-622.

[5] Inoue, T., Teruya, Y. and Monde, M., Enhancement of pool boiling heat transfer in water and ethanol/water mixtures with surface-active agent, *International Journal of Heat and Mass Transfer* 47 (2004) 5555-5563.

[6] Bonilla, C.F. and Perry, C.W., Heat transmission to boiling binary liquid mixtures, *Trans. AIChE*, 37(1941) 685-705.

]7] McGllis, W.M. and Carey, V.P., On the role of Marangoni effects on the critical heat flux for pool boiling of binary mixtures, *J. Heat Transfer*, 118(1996) 103-109.

[8] Sun, K.H. and Lienhard, J.H., The peak pool boiling heat flux on horizontal cylinders, *Int. J. Heat Mass Transfer*, 13(1970) 1425-1439.

[9] Hovestreudt,J., The influence of the surface tension difference on the boiling of mixtures, *Chem. Eng. Sci.*, 18(1963) 631-639.

[10] Yagov, V.V., Critical heat flux prediction for pool boiling of binary mixtures, *Chemical Engineering Research and Design*, 82(A4) (2004) 457-461.

[11] Ono, A. and Sakashita, H., Liquid-vapor structure near heating surface at high heat flux in subcooled pool boiling, *Int. J. Heat Mass Transfer*, 50(2007) 3481-3489.

[12] Hoke, B.C. and Chen, J.C., Binary aqueous-organic surface tension temperature dependence, *J. Chem. Eng. Data*, 36(1991) 322-326.

[13] Stephan, K. and Abdelsalam, M., Heat-transfer correlations for natural

convection boiling, *Int. J. Heat Mass Transfer*, 20(1980) 73-87.
[14] Ono, A. and Sakashita, H., Measurement of surface dryout near heating surface at high heat fluxes in subcooled pool boiling, *Int. J. Heat Mass Transfer*, 52(2009) 814-821.
[15] Iida,Y. and Kobayasi, K., An experimental investigation on the mechanism of pool boiling phenomena by a probe method, *Proc. 4th Int. Heat Transfer Conf.*, Paris, 5(1970) 1-11.
[16] Bhat,A.M, Prakash,R. and Saini,J.S., On the mechanism of macrolayer formation in nucleate pool boiling at high heat flux, *Int. J. Heat Mass Transfer*, 26-5(1983) 735-739.
[17] Haramura,Y. and Katto, Y., A new model of critical heat flux, applicable widely to both pool and forced convection boiling on submerged bodies in saturated liquids, *Int. J. Heat Mass Transfer*, 26-3(1983) 389-398.
[18] Rajvanshi,A.K., Saini, J.S. and Prakash, R., Investigation of macrolayer thickness in nucleate pool boiling*, Int. J. Heat Mass Transfer*, 35-2 (1992) 343-350.
[19] Chen,L., Mewes, D. and Luke, A., Boiling phenomena with surfactants and polymeric additives: A state-of the-art review, *International Journal of Heat and Mass Transfer*, 50(2007) 2744-2771.

Captions of Figures

Fig.1 Experimental apparatus.

Fig.2 Examples of probe signals.

Fig.3 Phase equilibrium diagram and surface tension of 2-propanol/water mixtures.

Fig.4 Boiling curves for water and 2-propanol/water mixtures.

Fig.5 Changes in CHF with concentration of 2-propanol.

Fig.6 Boiling behaviors for water and the 2-propanol/water mixture(3.0 mol%).

Fig.7 Vertical distributions of void fractions for water measured at the center of the heating surface.

Fig.8 Vertical distributions of void fractions for a 2-propanol/water mixture (3.0mol%) measured at the center of the heating surface.

Fig.9 Radial distributions of void fractions for water (q =1.3MW/m^2).

Fig.10 Radial distributions of void fractions for the 3.0mol% of 2-propanol/water mixture (q=1.5MW/m^2).

Fig.11 Frequency distributions of the 4-6, 18-20, and 36-38 ms-wide pulses

Fig.12 Pulse width spectrum and height of pulse disappearance.

Fig.13 Liquid layer thickness for water and the 2-propanol/water mixture (3.0mol%) measured at the center of the heating surface.

Fig.14 Radial distributions of liquid layer thicknesses of water and the 2-propanol/water mixture (3.0mol%).

Fig.15 Variation in liquid layer thickness vs. concentration of 2-propanol (measured at the center of the heating surface for heat fluxes of 1.58 to 1.64MW/m^2).

Fig.16 Boiling behaviors of SDS aqueous solution (600ppm).

Fig.17 Boiling curves of water, 2-propanol/water mixture (3.0mol%), and SDS aqueous solution (600ppm).

Fig.18 Vertical distributions of void fractions measured at the center of the heating surface for water, 2-propanol/water mixture (3.0mol%), and SDS

aqueous solution (600ppm).

Fig.19 Radial distributions of void fractions for SDS aqueous solution (600ppm).

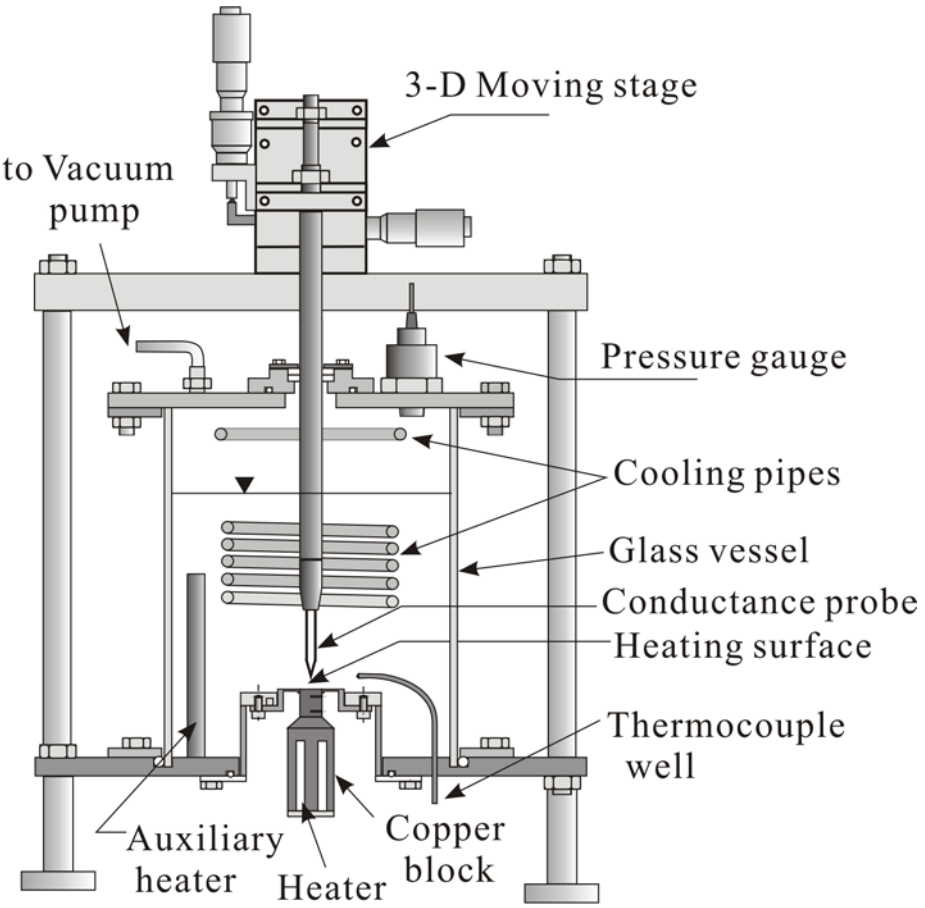

Fig.1 Experimental apparatus.

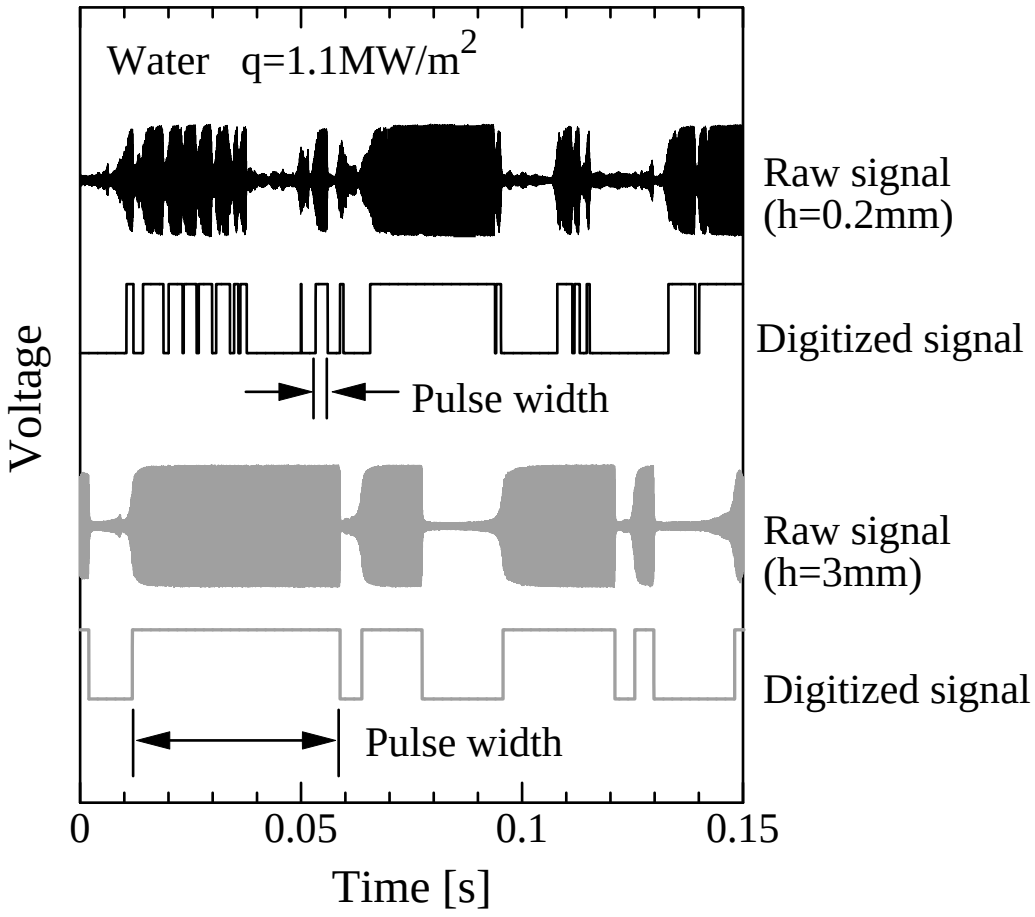

Fig.2 Examples of probe signals

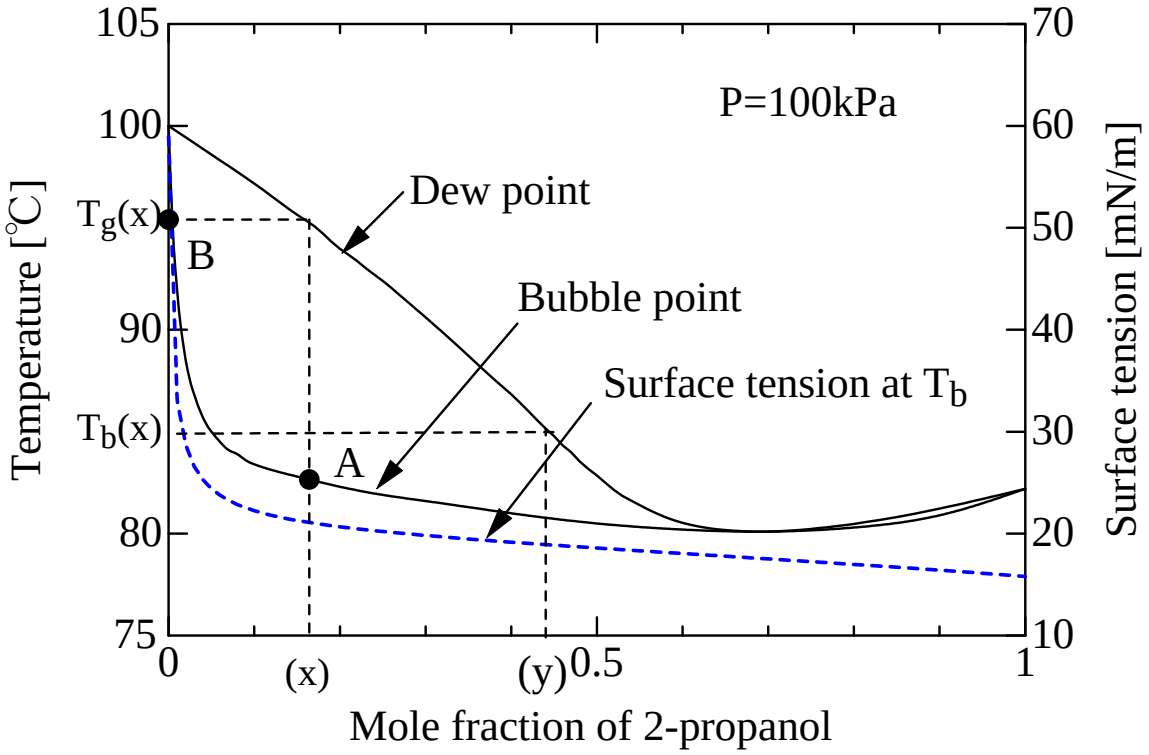

Fig.3 Phase equilibrium diagram and surface tension of 2-propanol/water mixtures

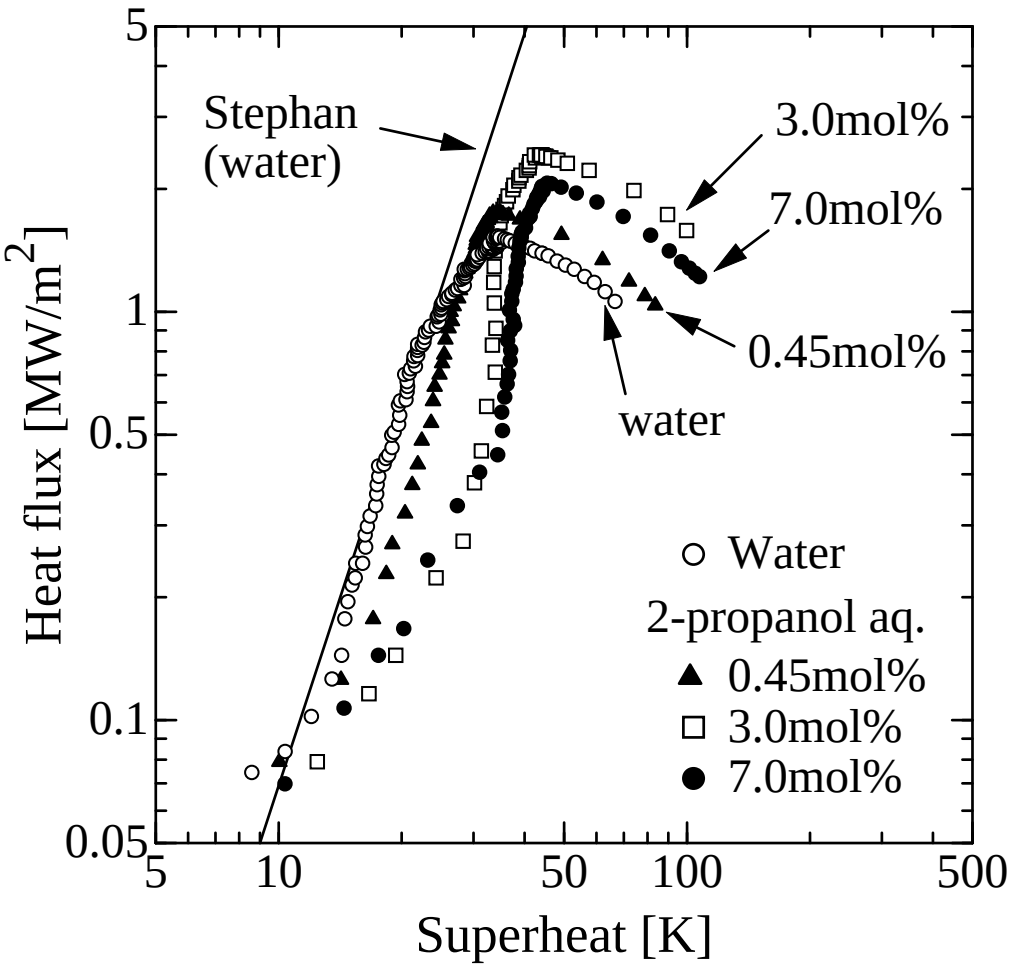

Fig.4 Boiling curves for water and 2-propanol/water mixtures

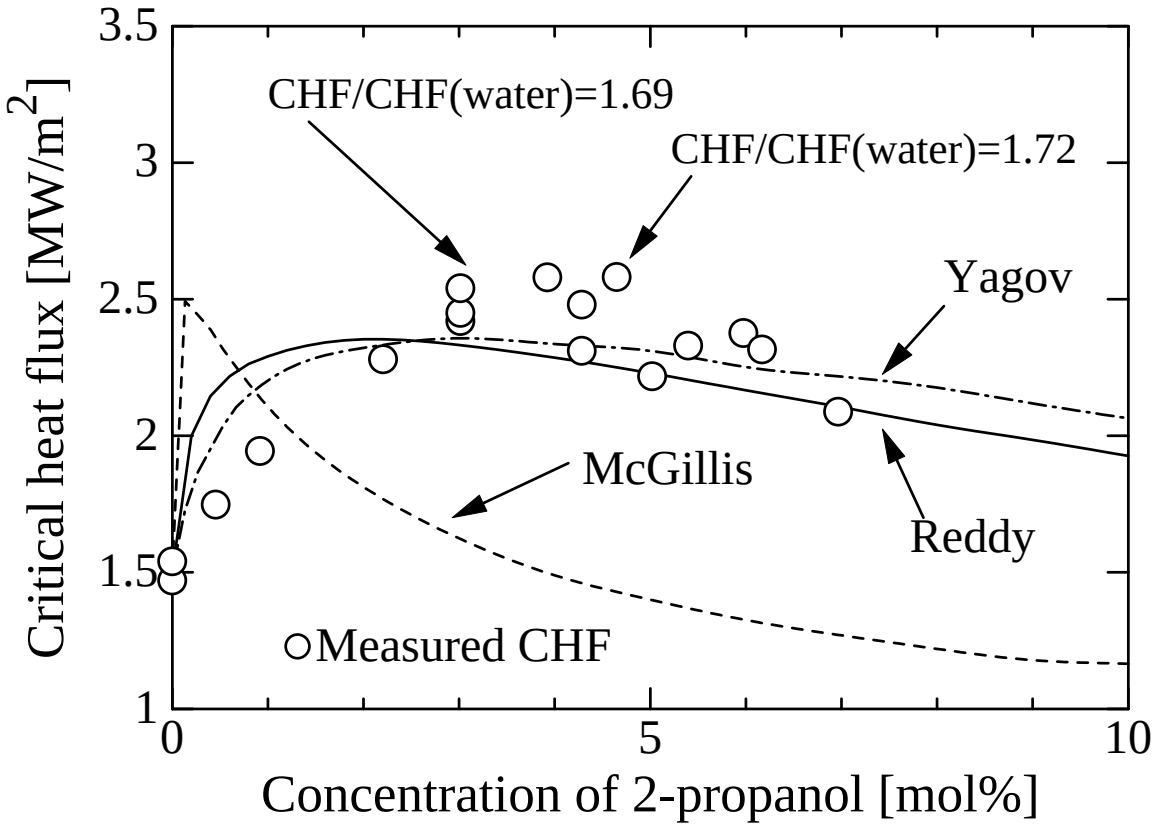

Fig.5 Changes in CHF with concentration of 2-propanol

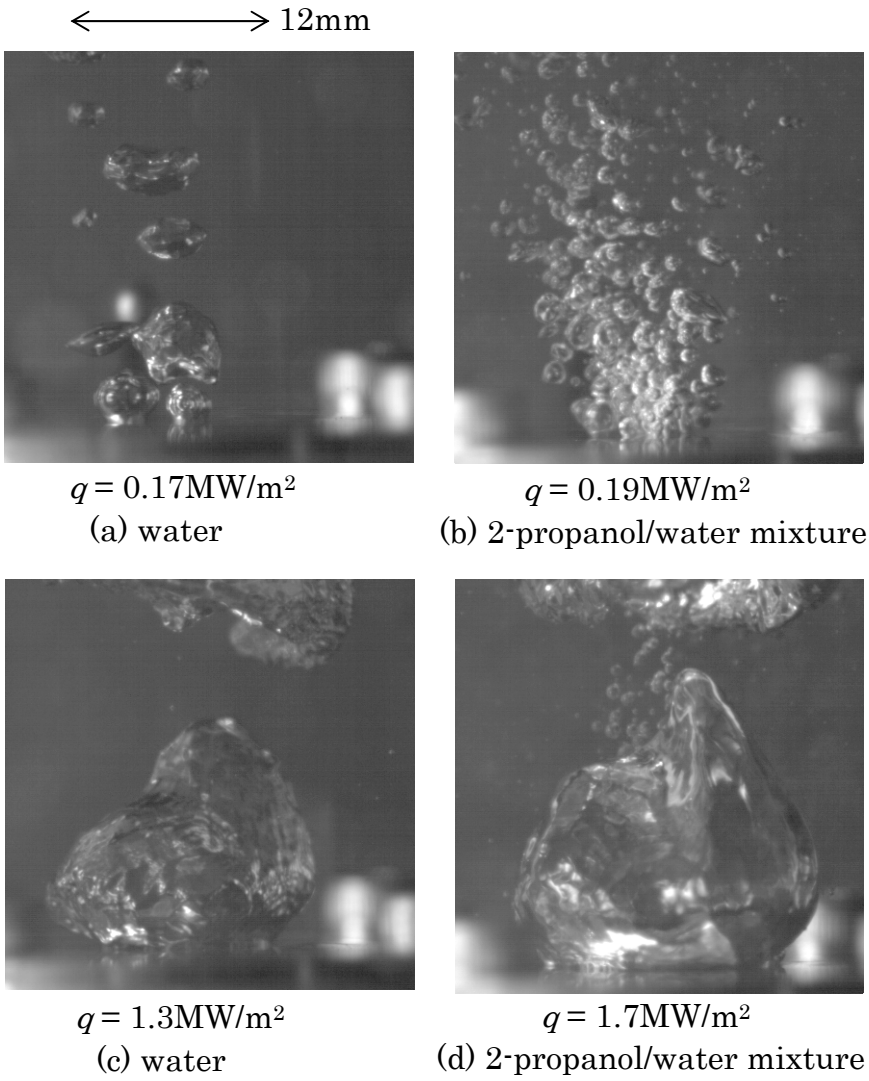

Fig.6　Boiling behaviors for water and the 2-propanol/water mixture (3.0 mol%)

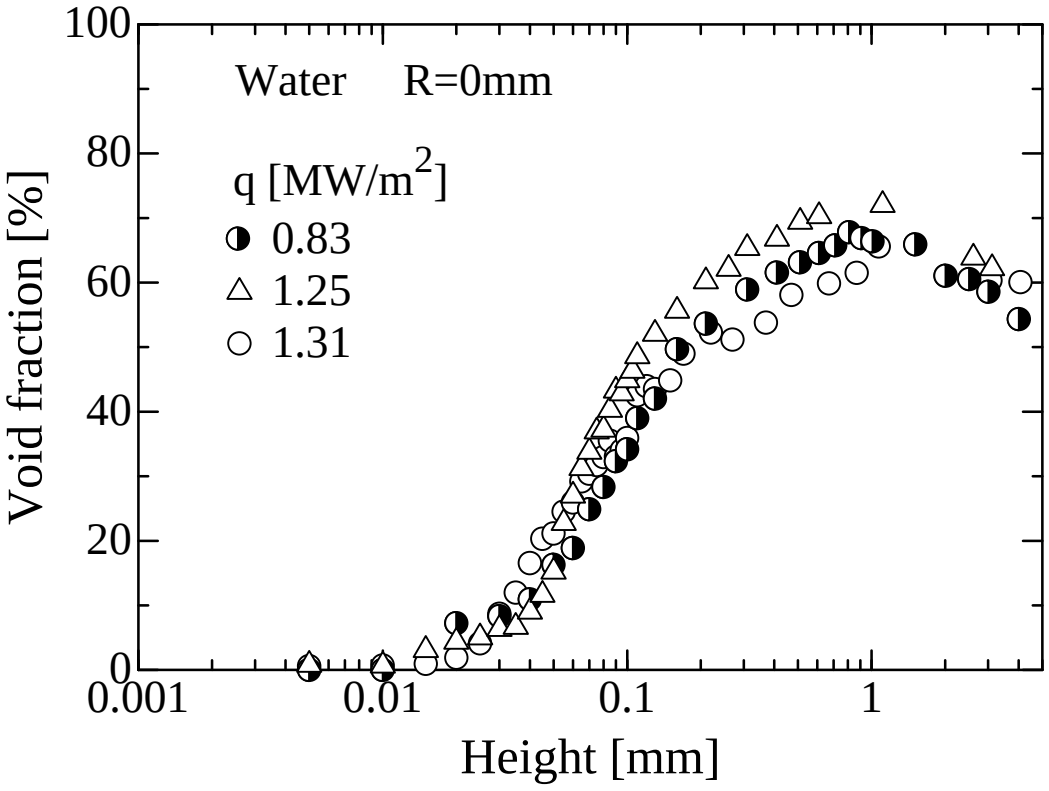

Fig.7 Vertical distributions of void fractions for water measured at the center of the heating surface

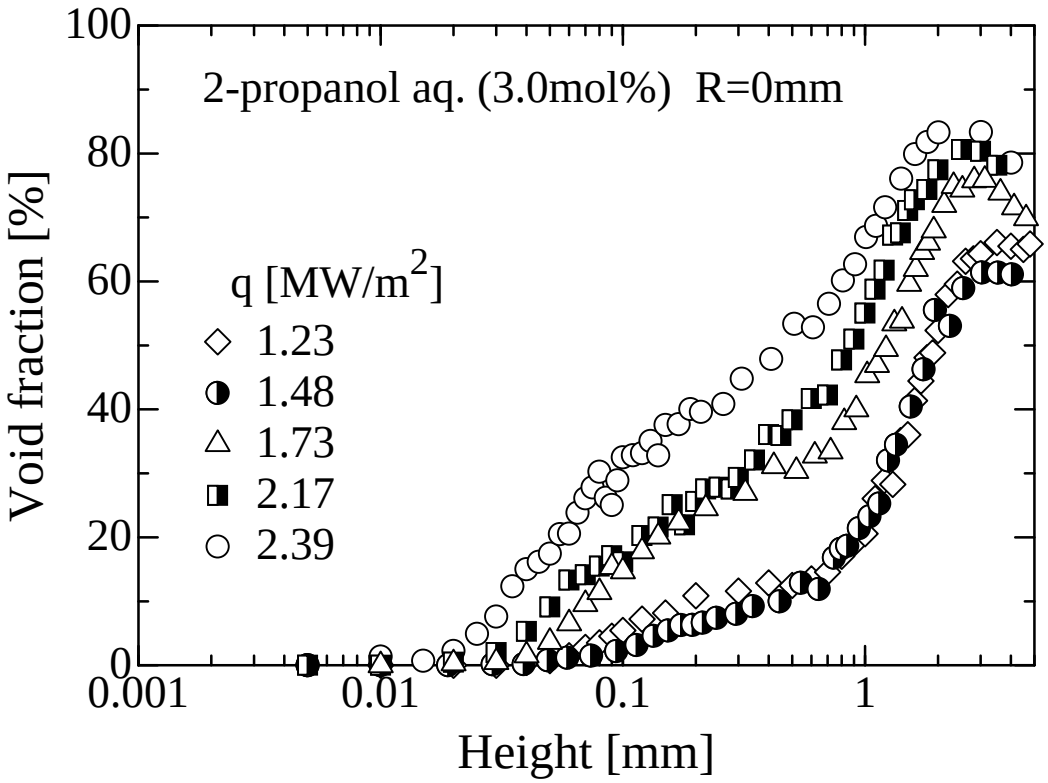

Fig.8 Vertical distributions of void fractions for a 2-propanol/water mixture (3.0 mol%) measured at the center of the heating surface

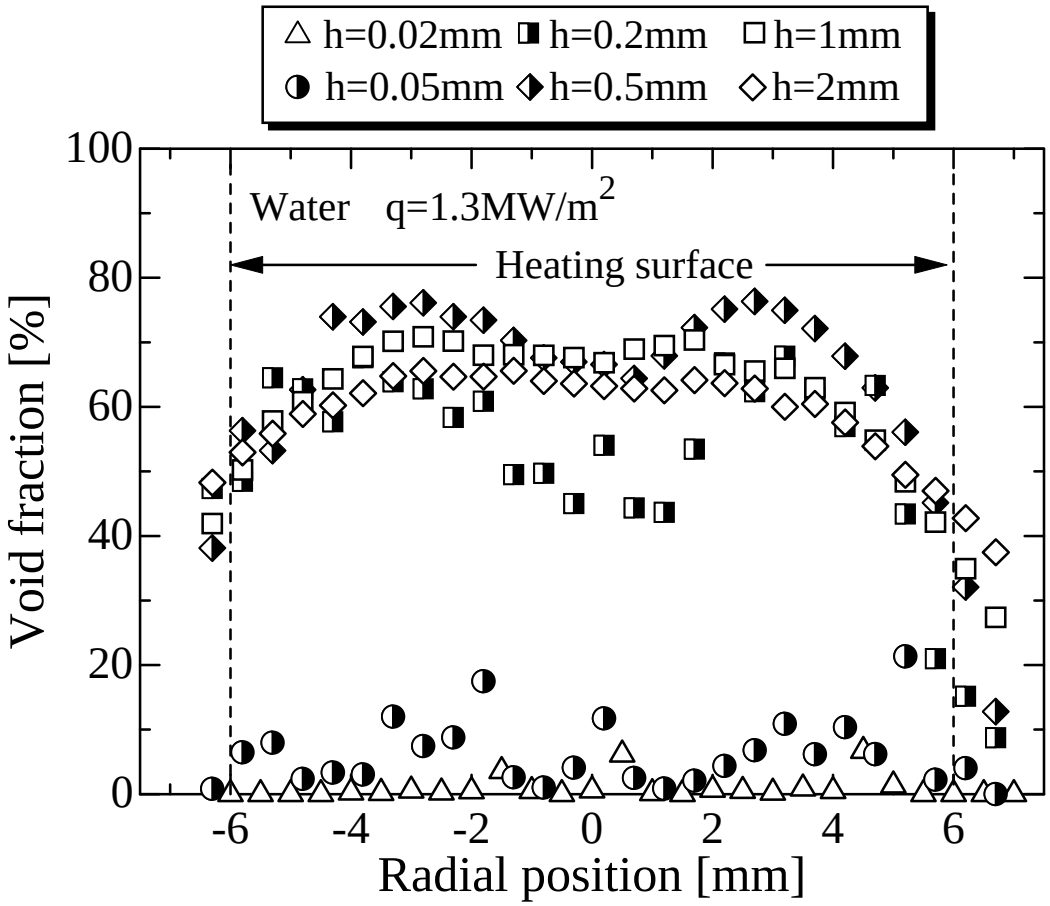

Fig.9 Radial distributions of void fractions for water (q =1.3MW/m^2)

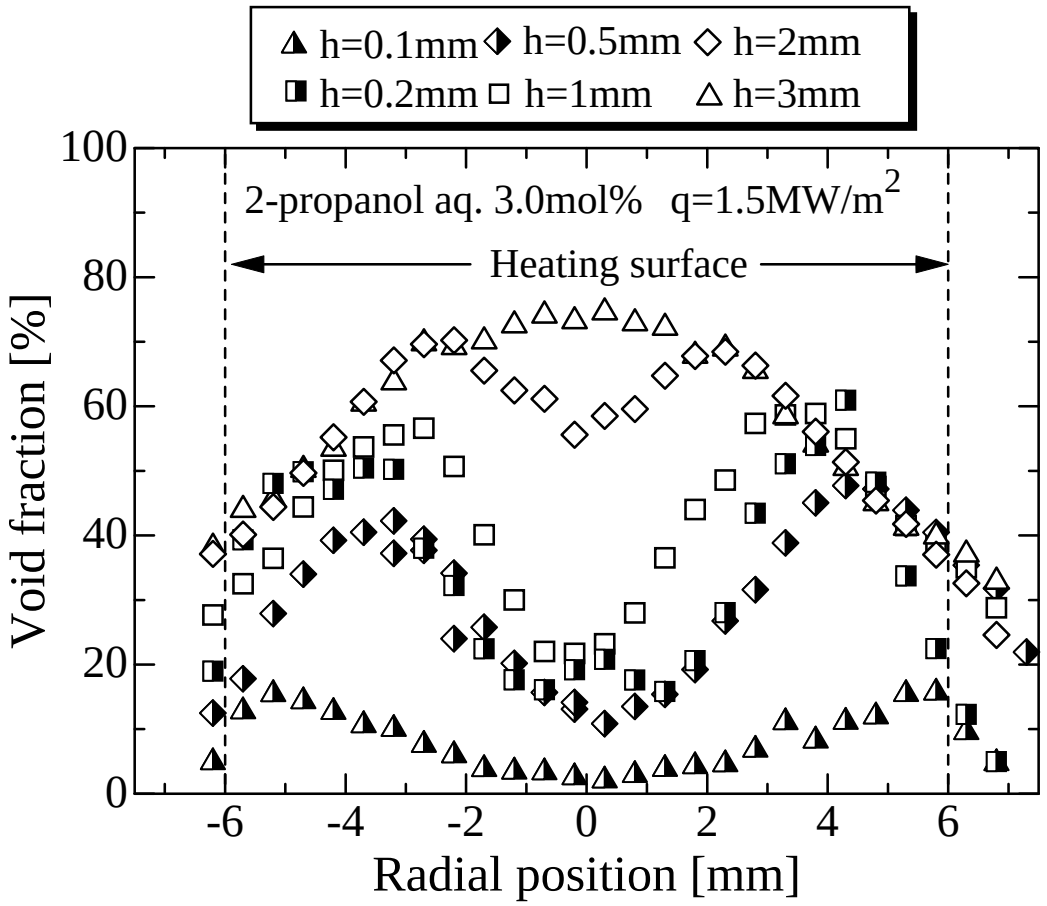

Fig.10 Radial distributions of void fractions for the 3.0mol% of 2-propanol/water mixture (q=1.5MW/m^2)

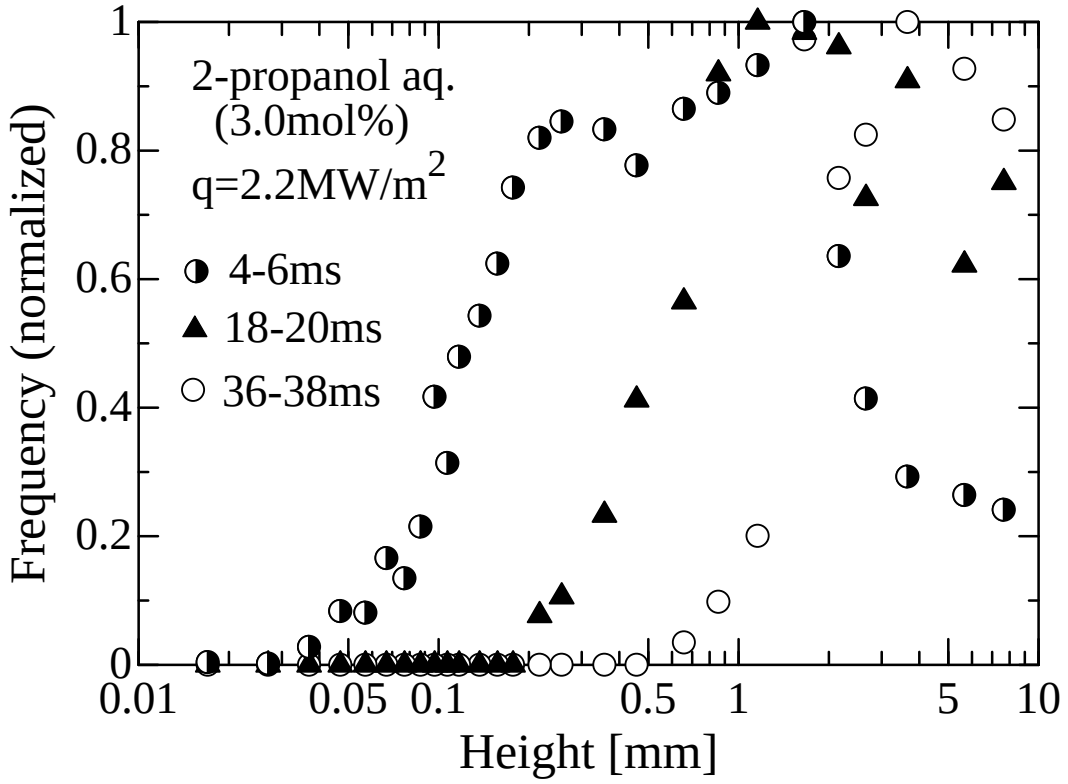

Fig. 11 Frequency distributions of the 4-6, 18-20, and 36-38 ms-wide pulses

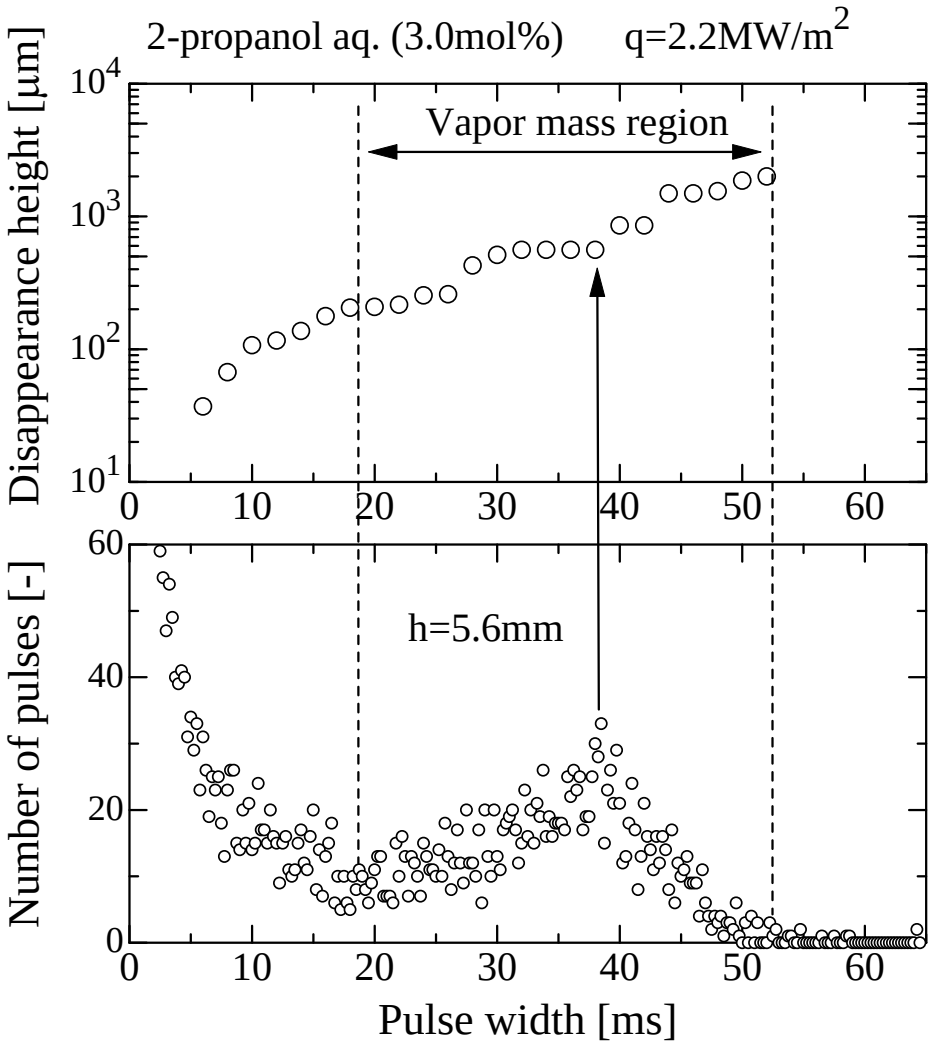

Fig.12 Pulse width spectrum and height of pulse disappearance

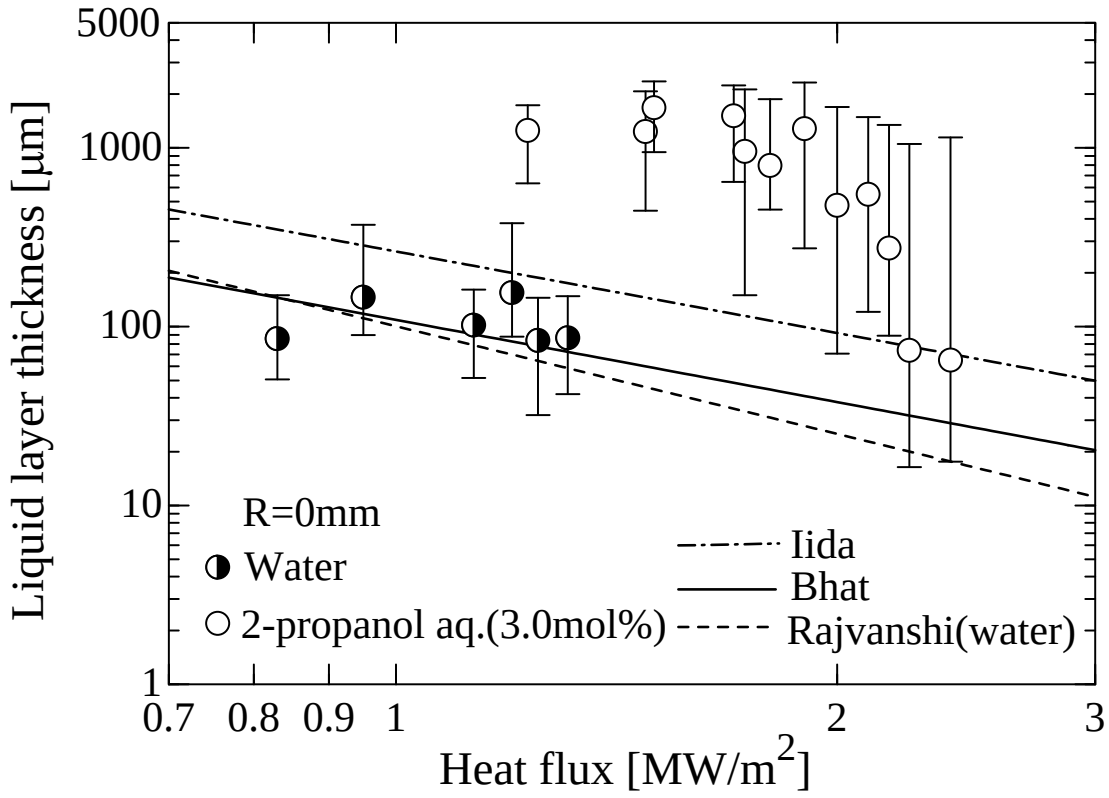

Fig.13 Liquid layer thickness for water and the 2-propanol/water mixture (3.0 mol%) measured at the center of the heating surface

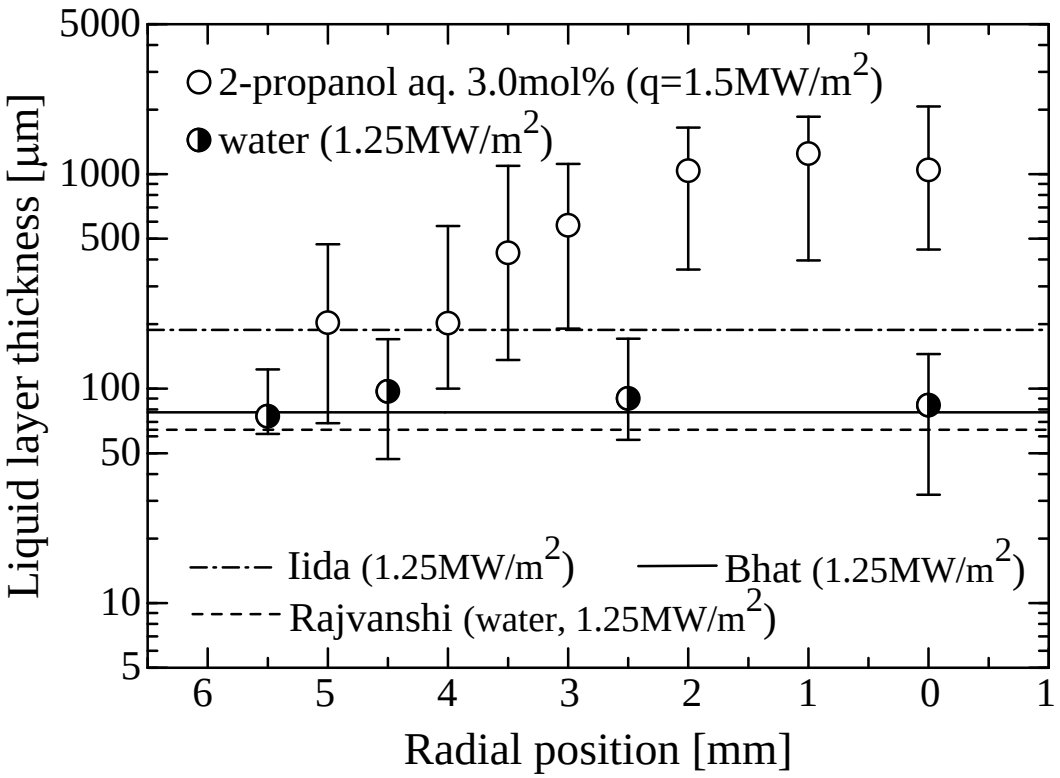

Fig.14 Radial distributions of liquid layer thicknesses of water and the 2-propanol/water mixture (3.0 mol%)

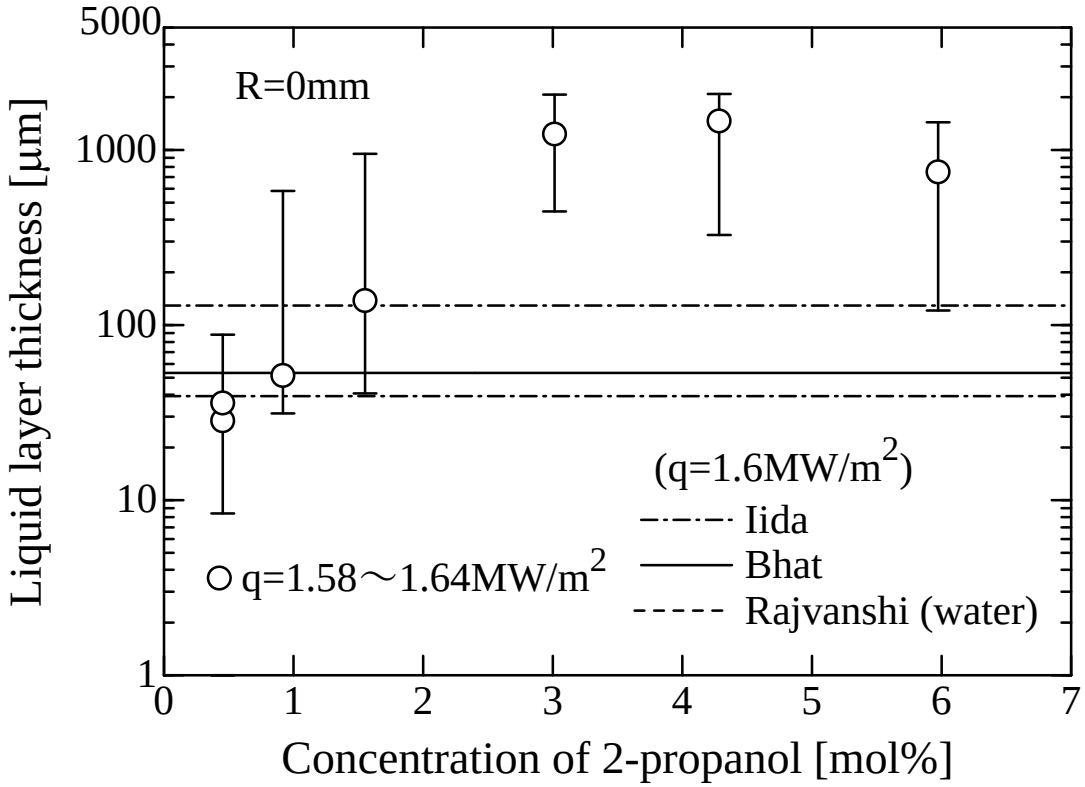

Fig.15 Variation in liquid layer thickness vs. concentration of 2-propanol (measured at the center of the heating surface for heat fluxes of 1.58 to 1.64MW/m2)

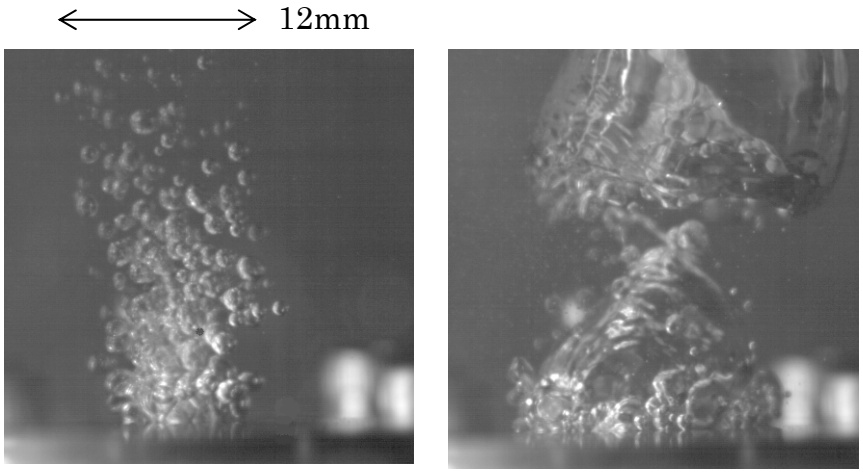

(a) q = 0.19MW/m^2 (b) q = 1.42MW/m^2

Fig.16 Boiling behaviors of SDS aqueous solution (600ppm)

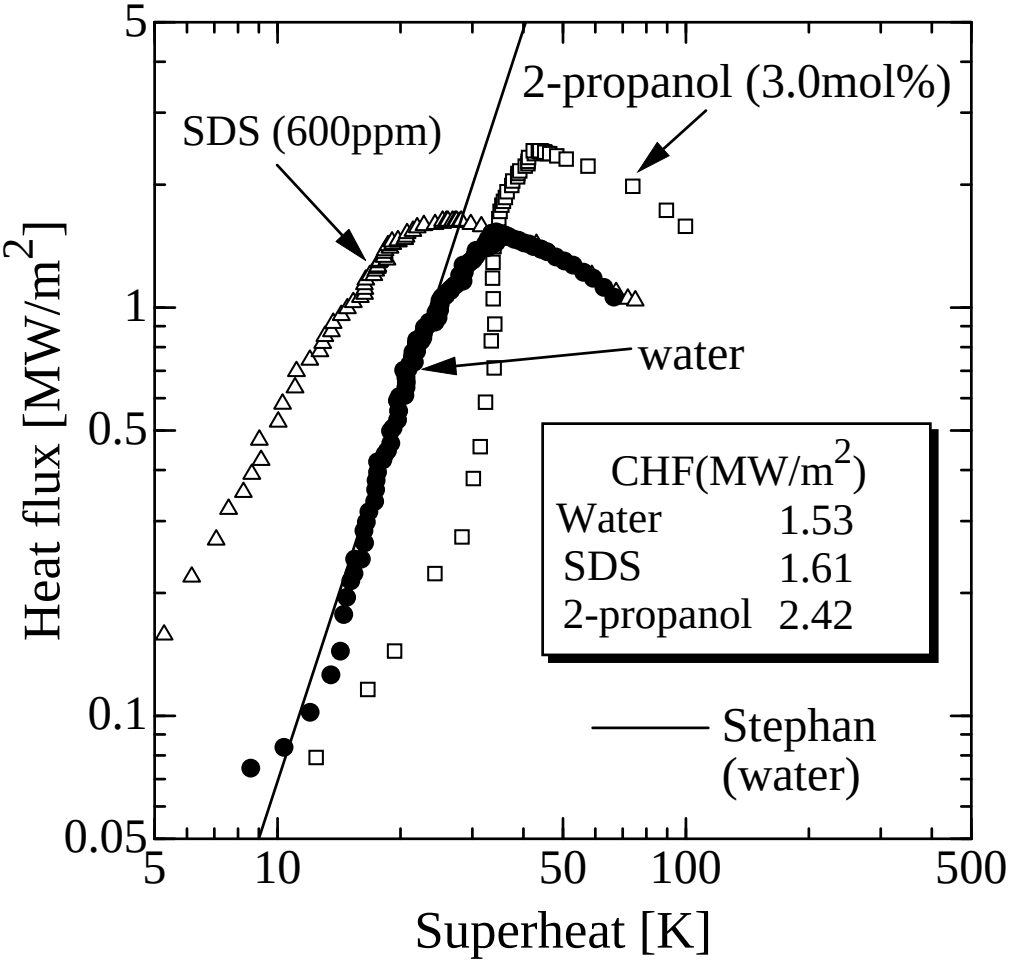

Fig.17 Boiling curves of water, 2-propanol/water mixtute (3.0 mol%), and SDS aqueous solution (600ppm)

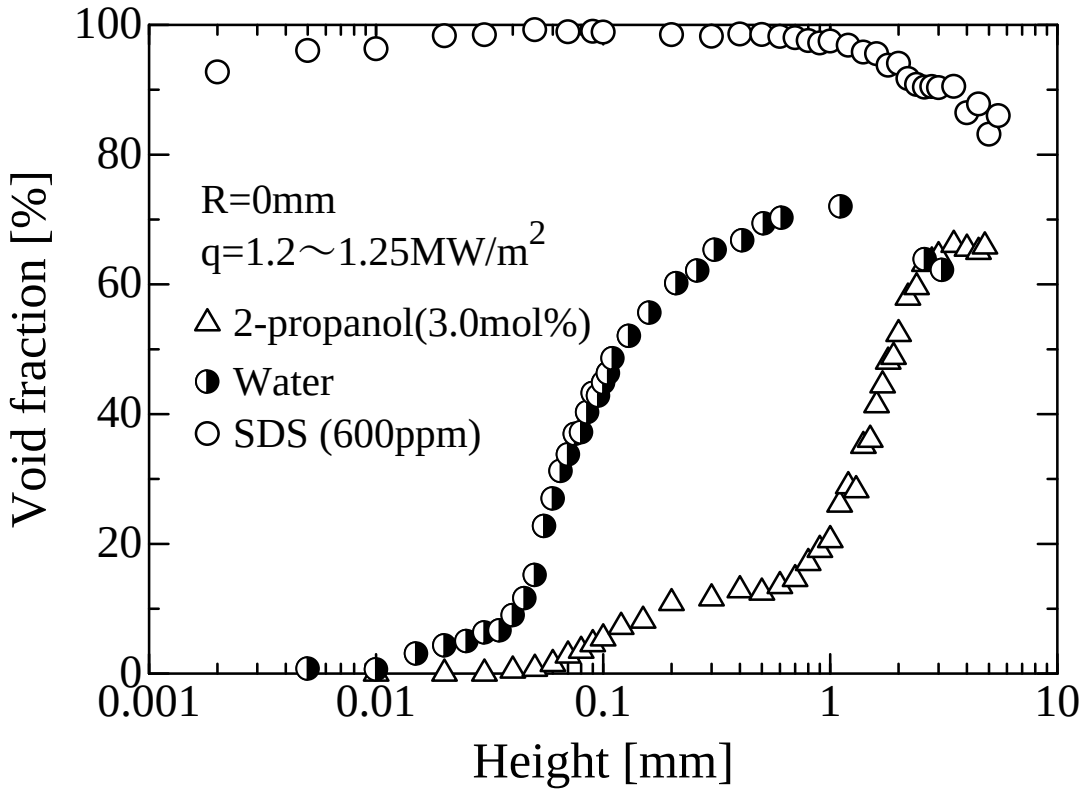

Fig.18 Vertical distributions of void fractions measured at the center of the heating surface for water, 2-propanol/water mixture (3.0mol%), and SDS aqueous solution (600ppm)

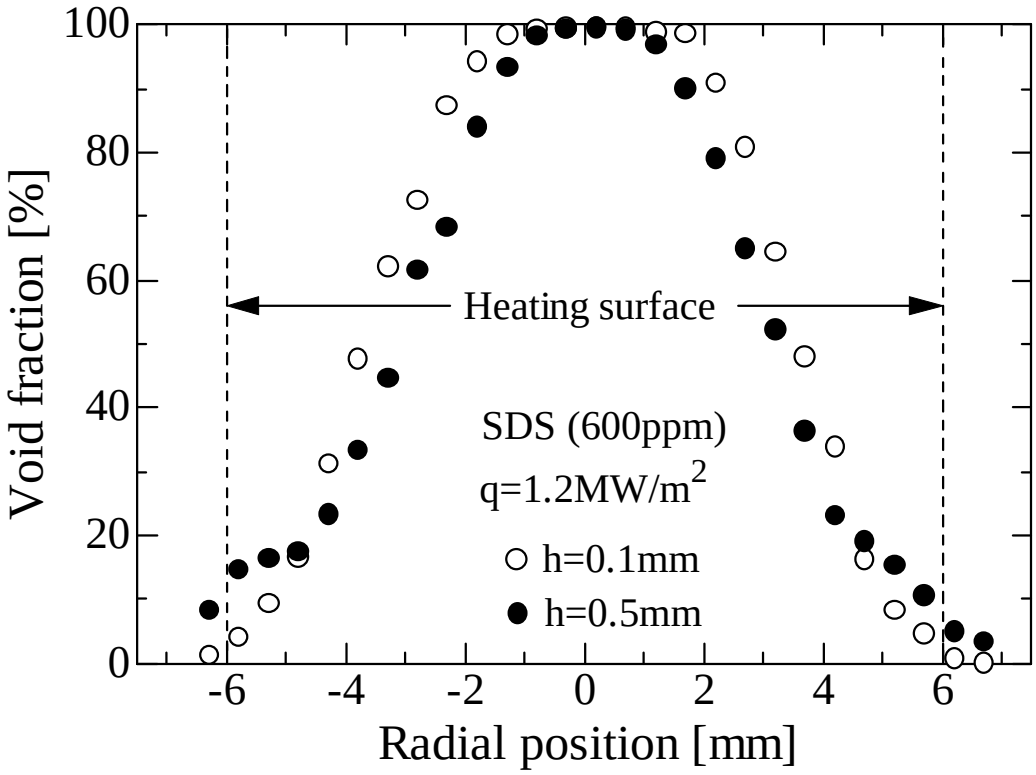

Fig.19 Radial distributions of void fractions for SDS aqueous solution (600ppm)